EFDA–JET–CP(12)04/12

P.C. de Vries, G. Arnoux, A. Huber, J. Flanagan, M. Lehnen, V. Riccardo, C. Reux, S. Jachmich, C Lowry, G. Calabro, D. Frigione, M Tsalas, N. Baumgarten, S. Brezinsek, M. Clever, D. Douai, M. Groth, T.C. Hender, E. Hodille, E. Joffrin, U. Kruezi, G.F. Matthews, J.A. Morris, R. Neu, V. Philipps, G. Sergienko, M. Sertoli and JET EFDA contributors

# The Impact of the ITER-Like Wall at JET on Disruptions

# The Impact of the ITER-Like Wall at JET on Disruptions

P.C. de Vries[1], G. Arnoux[2], A. Huber[3], J. Flanagan[2], M. Lehnen[3], V. Riccardo[2], C. Reux[4], S. Jachmich[5], C Lowry[6], G. Calabro[7], D. Frigione[7], M Tsalas[1], N. Baumgarten[3], S. Brezinsek[3], M. Clever[3], D. Douai[8], M. Groth[9], T.C. Hender[2], E. Hodille[10], E. Joffrin[8], U. Kruezi[3], G.F. Matthews[2], J.A. Morris[2], R. Neu[11], V. Philipps[3], G. Sergienko[3], M. Sertoli[10] and JET EFDA contributors*

***JET-EFDA, Culham Science Centre, OX14 3DB, Abingdon, UK***

*[1]FOM institute DIFFER, Association EURATOM-FOM, P.O.Box 120, Nieuwegein, Netherlands*
*[2]EURATOM-CCFE Fusion Association, Culham Science Centre, OX14 3DB, Abingdon, OXON, UK*
*[3]Institut für Energie-und Klimatforschung-IEK-4, Forschungszentrum Jülich GmbH, EURATOM Association, 52425 Jülich, Germany*
*[4]Ecole Polytechnique, CNRS, 91128 Palaiseau Cedex, France*
*[5]Association EURATOM-Etat Belge/Belgische Staat, ERM-KMS, Brussels, Belgium*
*[6]European Commission, Brussels, Belgium*
*[7]Associazione EURATOM/ENEA sulla Fusione, CP 65-00044 Frascati, Rome, Italy*
*[8]CEA, IRFM, F-13108 St-Paul-Lez-Durance, France*
*[9]Aalto University, Association EURATOM-Tekes, Espoo, Finland*
*[10]Ecole Central Lyon, 36 Avenue Guy de Collongue, 69134 Ecully Cedex, France*
*[11]Max-Planck-Institut für Plasmaphysik, EURATOM-Association, 85748 Garching, Germany*
** See annex of F. Romanelli et al, "Overview of JET Results", (23rd IAEA Fusion Energy Conference, Daejon, Republic of Korea (2010)).*

Preprint of Paper to be submitted for publication in Proceedings of the
39th European Physical Society Conference on Plasma Physics, Stockholm, Sweden
2nd July 2012 - 6th July 2012

**ABSTRACT**

The new full-metal ITER-like wall at JET was found to have a profound impact on the physics of disruptions. The main difference is a significantly lower fraction (by up to a factor of 5) of energy radiated during the disruption process, yielding higher plasma temperatures after the thermal quench and thus longer current quench times. Thus a larger fraction of the total energy was conducted to the wall resulting in larger heat loads. Active mitigation by means of massive gas injection became a necessity to avoid beryllium melting already at moderate levels of thermal and magnetic energy (i.e. already at plasma currents of 2MA). A slower current quench however reduced the risk of runaway generation. Another beneficial effect of the ITER-like wall is that disruptions have a negligible impact on the formation and performance of the subsequent discharge.

## 1. INTRODUCTION

The occurrence of Tokamak disruptions is a key issue for ITER and could restrict its operational capabilities. In such events a rapid loss of the thermal energy followed by a quench of the plasma current results in large heat loads and electromagnetic forces on surrounding structures [1]. Furthermore, disruptions usually cause significant de-conditioning, affecting the performance of subsequent discharges. Hence, considerable efforts have been devoted to understanding the physics of disruptions; what causes them, how they can be avoided [2, 3, 4], their impact [5, 6, 7] and how to mitigate the effects [8, 9, 10, 11].

In all these aspects the recent replacement of Carbon (C) Plasma-Facing Components (PFC) with a metallic wall provided new challenges for the operation of JET. The ITER-Like Wall (ILW) consists of beryllium (Be) tiles in the main chamber and both bulk tungsten (W) and tungsten-coated tiles in the divertor [12]. The tolerable heat loads with the new wall are more restricted, with melting occurring already for heat loads of ~20MJm$^{-2}$s$^{-1/2}$ for Be and at ~50MJm$^{-2}$s$^{-1/2}$ for W [13]. For Be the melt limit will already be reached for a fast quench (~2.5ms) of 1MJ thermal energy. About half of the magnetic energy is usually coupled back into the toroidal conducting structures such as the vacuum vessel or poloidal field coils [14], hence the other half can heat plasma facing components. As an example, at a plasma current of $I_p$ = 2MA about 9MJ of magnetic energy is available which if quenched in 50ms and deposited on typically 1m$^2$ could cause Be melting. This is a worst case estimate because the wetted area can be larger. Moreover, for C PFCs a significant part of this energy is usually can be radiated. Nevertheless it raises the question of how much more vulnerable the ILW is to damage by disruption heat loads.

Another intriguing question is, whether the change of the plasma-facing material itself can significantly affect the physics of disruptions. Changes in density or radiation control may also create new problems (i.e. new disruption causes) yielding a higher disruption rate [4]. Moreover, recycling and impurities are known to play a role in the physics of the density limit [15, 16, 17]. In section 2 a summary of the first studies on the impact of the ILW on disruption causes will be given. Next, in section 3, the effect of the ILW on the dynamics of the disruption process itself will be presented. Previous operations with Be main chamber belt limiters at JET already showed

a considerable slower current quench time compared to operations with C PFC [18]. The reasons for this difference and the consequences for heat loads, vessel forces as well as the efficiency of mitigation by massive gas injection will be discussed. Section 4, will compare out-gassing and deconditioning by disruptions with C PFCs and the ILW and will analyse the impact on the formation and performance of following discharges. Despite the vulnerability of the new PFC, intentional disruption studies featured heavily in the first experimental programme carried out with the ILW, in order to answer these issues. The main conclusions will be summarized in the final section.

## 2. DISRUPTIONS CAUSES AND THE ITER-LIKE WALL

Over the last few years of operation with C PFCs, the (unintentional) disruption rate was found to drop significantly to a relatively low level of about 3.4% just before the installation of the new ILW [4]. First operations with the new ILW broke this trend, with an increased disruption rate; from August 2011 until mid of June 2012 about 2300 plasma discharges (with $I_p > 1$MA) have been run, of which 8.6% disrupted unintentionally, more than twice the previous rate. Moreover, the later part of period, which featured high performance operations, showed a disruption rate of 10-15%. To add to this, a large number of disruptions were carried out intentionally because assessment of disruptions loads was key to expanding of the operational range with the new wall, bringing the total disruptions rate to 13.2%.

### *2.1 NEW CAUSES OF DISRUPTIONS*

A more detailed study into the impact of the ILW on disruption causes is ongoing but two main differences are clear. Firstly, the ILW altered the density control; hence, recipes tuned during C wall operations did not work anymore and had to be retuned. Transient wall pumping by the Be mainchamber PFCs resulted in several cases in too low a density and error field locked modes. Most issues with density feedback were brought under control during the first 3 months of operation. Secondly, more disruptions were caused by strong accumulation of impurities, originating from W sputtering, while also direct influx of W and Ni micro-particles has been observed. Tungsten sputtering is determined mainly by the divertor plasma temperature and impurity content [19]. Control of the impurity accumulation and peaking proved to be difficult, leading to strongly peaked impurity density and radiation profiles. This is similar to strong density peaking seen with the previous C PFC that could eventually lead to a radiative collapse [4]. With the ILW the core radiation can be strong enough to cause hollow temperature profiles.

A typical example is shown in figure 1, where W accumulation occurs during the step-down of auxiliary Neutral Beam Injection (NBI) power. Early signs are a change in sawtooth activity (seen here as a reduction in the $n = 1$ sawtooth precursor) and an increasing radiation from about $t = 22.5$s. Soon after this strong W lines can be observed by VUV spectroscopy and the temperature profile becomes hollow with a core temperature decreasing below $T_e = 370$eV. Most likely this affects the current density profile and the associated Magneto HydroDynamic (MHD) activity is reminiscent of observations in other devices [20]. An MHD precursor instability (with a toroidal mode number $n = 1$)

eventually creates a locked mode, at t = 23.845s, causing a first thermal quench (and typical current spike). Instead of leading to a full disruption of the plasma, it actually results in a flushing of the core impurities and an increase of the core temperature back to a maximum of $T_e = 1.7$keV. These very high post thermal quench temperatures lead to a nearly negligible current quench rate. A quasi-stationary mode persists and a second thermal quench (and current spike) takes place at t = 24.898s. The plasma becomes vertically unstable thereafter and a further decrease in plasma temperature yields a faster current quench. The observations illustrate a few interesting points: the plasma improves after the thermal quench and the temperatures during the current quench may be high enough to slow it down significantly. The consequences of these slower current quenches will be discussed in the next section.

### *2.2 THE DENSITY LIMIT*

In tokamaks disruptions occur when the density is too high [21]. This well known operational limit has however little to do with the actual average plasma density and is more related to radiation instabilities that develop at the plasma edge. For increasing edge density the corresponding temperature decreases, increasing the radiation efficiency of typical impurities. The line-radiation eventually exceeds the local heating power with the result that below a specific temperature for a given impurity the edge temperature collapses. Deuterium recycling and re-ionization can also play a role in the cooling process of the plasma edge, becoming important when impurity concentrations are low [15]. The contraction of the plasma current profile due to the edge cooling eventually triggers MHD instabilities that cause the disruption. Two density limit disruptions with C PFCs and the ILW, respectively, are compared in figure 2. The main parameters of both ELMy H-mode discharges are similar; with $B_T = 3.1$T, $I_p = 2.0$MA, $q_{95} = 4.5$, using the same high triangularity configuration with $<\delta> = 0.42$ and comparable NBI heating powers $P_{NB} = 8$-10MW. The striking difference is that only 2.4barl of deuterium was injected in the plasma with C PFC while 11.4barl was needed to disrupt the plasma with the ILW. In the latter case a maximum gas dosing rate of $5.5\times10^{23}$ electrons/s was reached, >5 times more than in C.

The disruption process with C PFCs typically showed a back-transition from H to L-mode, detachment of the outer divertor, formation of an X-point and inner wall MARFE (i.e. localised radiation instabilities) that triggered MHD instabilities and eventually the disruption [21]. The inner divertor is usually already fully detached much earlier in the discharge. In figure 2 it can be seen that for C PFCs this whole process starts ~150-200ms before the disruption. The loss in confinement due to the H to L back-transition, usually leads to a drop in density due to the lower particle confinement in L-mode, thus the actual disruption takes place below the maximum achievable density. With the ILW the H to L back-transition and drop in density takes place 1.1s before the disruption. The maximum achievable density is set by a non-disruptive H-mode density-limit. The physics related to the confinement back transition is unlikely to be related to the events that eventually trigger the disruption in L-mode.

The exact limit at which the edge becomes unstable due to impurity radiation losses is of course determined by edge impurity content, as shown in figure 2, with the ILW C influx was found to be

more than one magnitude lower [23]. The beryllium content of ILW plasmas which results from physical sputtering decreases strongly at high densities. It was observed that the onset of the radiation instability or MARFE occurred with the ILW at a significantly lower edge temperature [22]. For ILW edge plasmas the main radiators can be considered D and Be. Because the radiation efficiency for Be is about a factor of 10 lower than for C and the optimum radiation temperature is ~2eV compared to ~10eV for C, the radiation instability develops at much lower temperatures. This makes it possible to operate at higher edge (and line-averaged) densities with the ILW with the ultimate limit probably dominated by radiation from deuterium related species [22].

## 3. IMPACT ON CURRENT QUENCH, FORCES AND HEAT LOADS

In figure 2 another important difference is the substantially longer current quench time for the disruption with the ILW. The observation in figure 2 is quite representative and in figure 3 the statistics of current quench times is shown for a large number of C PFC and ILW cases. For JET, the current quench time can range from several tens to hundreds of milliseconds. Here, the normalised current quench times are defined as 5/3 of the time it takes to reduce the current from 80% of its predisruption value to 20%, divided by the plasma cross-section area. The figure shows that the current quench times are systematically longer for the ILW and 49% of disruptions have a normalised current quench time of $5/3\ t_{80-20}/S > 19$ ms m$^{-2}$ compared to 5.8% for C PFC disruptions. Only 4.2% of the ILW disruptions have a normalised current quench time below 5ms m$^{-2}$ (these were almost all Vertical Displacement Events (VDEs)), contrasting with 45% of C PFC disruptions. Some of the very slow current quench cases exhibit multiple thermal quenches and current spikes, each in turn stepwise reducing the plasma temperature.

Dissipation of both thermal and magnetic energy during a disruption can be described by a set of coupled differential equations:

$$\frac{dE_{mag}}{dt} = P_{coupled} - P_{OH} - P_{RE} \tag{1}$$

$$\frac{dE_{therm}}{dt} = P_{OH} - P_{cond} - P_{rad} \tag{2}$$

$$\frac{dE_{RE}}{dt} = P_{RE} - P_{cond}^{RE} - P_{rad}^{RE} \tag{3}$$

The (poloidal) magnetic energy can be dissipated by Ohmic Heating ($P_{OH}$), induced by poloidal field coils but also coupled back into toroidal conductors via transformer action ($P_{coupled}$), as described in ref. [14], or by accelerating electrons to relativistic velocities forming so-called runaway electron beams. Heat loads due to such runaway electrons could pose a serious threat to the PFCs [1, 25]. The power coupled back to external circuits and structures during the current quench phase is not negligible and usually between 40% and 50% of the magnetic energy is dissipated in this way. The

thermal and runaway electron energy can be conducted directly to the PFC ($P_{cond}$). Part of the thermal energy will be radiated (Prad). Neglecting runaways, equation 1 is the energy form of Ohm's law,

$$L \frac{dI_p}{dt} = \vec{M} \cdot \frac{d\vec{I_T}}{dt} - I_p R \tag{4}$$

The first part on the right-hand-side is the flux provided by the poloidal field coils to drive the plasma current (i.e. the loop voltage) but also the coupling of current or plasma energy back into these coils or any other toroidal conductors such as the vacuum vessel during a current quench due to the mutual inductance, M. Here IT are the currents flowing in these conductors. It is clear that the current quench duration relates to the L/R time of the plasma, the ratio of the plasma inductance, L (for JET approximately 4μH), and its resistance, R, and hence should scale, assuming Spitzer, as $Z_{eff}^{-1}$ $<T_e>^{3/2}$, where $Z_{eff}$ and $<T_e>$ are the average effective charge and electron temperature, respectively [24]. If one neglects the mutual inductance, it is easy to calculate that a current quench time lower than 27ms would correspond to temperatures as low as $<T_e>$~5eV (for $Z_{eff} = 4$) while those above 154ms would suggest temperatures above $<T_e>$~40eV.

The radiation during disruptions with the ILW was found to be lower compared to the levels found during C PFC disruptions. Note that lower post-thermal quench temperatures for C PFC are not only the result of the higher radiation but are also enhancing the impurity radiation efficiency. For the two cases shown in figure 2, a total of $E_{rad} = 3$MJ is radiated during the disruption with the C PFC, which contrasts to $E_{rad} = 1.5$MJ with the ILW. Both cases have an identical magnetic energy of $E_{mag} = 10$MJ and similar thermal energy $E_{therm}$~1MJ at the time of the thermal quench. Figure 4a shows a direct correlation between the duration of the current or magnetic energy quench and the fraction of energy that is radiated. For C PFC the heat load due to the thermal quench may have released more C into the remaining plasma, with post-thermal quench temperatures close to the optimum temperature for C radiation (~10eV). Hence further cooling by line-radiation losses, and the onset of a densitylimit disruption, can be expected [13]. For the ILW radiation losses are not dominant and the temperature after the thermal quench may settle at higher values (i.e. >>100eV), well above the optimum for Be line-radiation. As shown in figure 1 the temperature may even increase again after a thermal quench.

The higher post-thermal quench temperature, lower $Z_{eff}$, and thus longer current quench time has several consequences. Firstly, a slower reduction in plasma current reduces eddy currents in the surrounding conductors and thus lowering the resulting eddy current forces. Moreover, a slower quench of plasma current induces a smaller toroidal electric field. This electric field can accelerate electrons to high energies, so called runaway electrons. Experiments have so far shown that disruptions that produced runaways with C PFC, do not create any when repeated with the ILW. This suggests that the longer current quench lowered the toroidal electric field below the level critical to generate runway electrons. The latter also depends on $Z_{eff}$ and $T_e$ but scales as $Z_{eff}\, T_e^{-1}$ [25]. It should be said that this result does not exclude the formation of runaway beams with an ILW, but merely makes them less likely.

### *3.1. DISRUPTION HEAT LOADS*

During disruptions with the ILW a smaller fraction of the total energy is radiated, and thus a larger fraction is directly conducted to the wall. Figure 4b also shows that for C PFC disruptions up to 100% of the energy that is not coupled back into the poloidal field coils was radiated. This contrasts with the ILW where never more than 50% is radiated. This is especially true for VDEs that make early contact and have shown radiation fractions as low as 10% of the total energy. It is obvious from the calculations presented in the introduction that this could lead to melt damage. It should be noted that the magnetic energy is more slowly dissipated due to the longer current quench with the ILW, however this is not sufficient to compensate for the larger fraction of conducted energy.

For the density-limit disruptions shown in figure 2, both high triangularity configurations become vertically unstable after the thermal quench and interact with the upper part of the vessel. The peak and average temperatures measured by a fast Infra-Red camera are shown in figure 5. The temperatures found for the ILW case are significantly higher with an increase of $\Delta T = 450°C$ reaching a peak temperature while the comparable C PFC case had $\Delta T \sim 210°C$. As mentioned above a significant higher fraction of the total energy was radiated during the C PFC current quench.

Added to figure 5 is an example of an intentionally triggered upward VDE. The plasma configuration is similar to the other two discharges, though the plasma has a lower total energy content of $E_{mag} + E_{therm} = 5.5 + 2.2 = 7.9MJ$ prior to the disruption. Nearly 49% of the magnetic energy was coupled back into the toroidal conductors but only 0.6MJ of it was radiated, remaining 4.3MJ to be directly conducted to the PFCs. Peak temperature exceeding the Be melt limit (1287°C) were measured in these cases in the upper part of the vessel. In-vessel video inspection following these experiments showed signs of Be melting on protection tiles near the top of the machine. It should be noted that peak temperatures obtained by these events depends strongly on the detailed interaction between the plasma and the PFC. Reshaping of the plasma configuration and movements of the contact point could spread the heat loads and lead to strong asymmetries in the deposition and thus temperature patterns on, for example, the upper protection tiles. It is therefore not straightforward to connect peak temperatures with the average heat loads expected during a disruption [7, 27]. Detailed analysis showed that the total power load in the upper part of the vessel due to such disruptions scaled with the available total pre-disruption energy [27].

### *3.2. DISRUPTION FORCES*

Electromagnetic forces are exerted on the vessel, either by eddy currents, induced by the plasma current decay and displacement, or by so-called halo currents, that run from the plasma through surrounding conductors it is touching [5]. Larger halo currents can be generated if the plasma touches early in the current quench phase. Hence, if the plasma moves vertically faster (i.e. a faster vertical growth rate) than the plasma current drops (i.e. a slow current quench), the fraction of plasma current in the halo is expected to be higher [5]. While lower halo fractions can be obtained even with slow current quenches, as long as the vertical growth rate is slower [28]. This is for example the case for

the example shown in figure 1, which has a very slow current quench and a maximum halo fraction of not more than 5% of the pre-disruption current. The overall picture found with the ILW is that no significant change in toroidal asymmetry with respect to the C PFC has been observed, though slightly higher halo fractions are obtained. In figure 6 the halo currents and vessel forces are shown for the two density limit disruptions discussed in the previous section (figure 2). The duration of the current quench is between 30 and 100ms for these two plasmas. The high triangularity plasma configuration $<\delta>=0.42$ has a high vertical growth rate ($\gamma \sim 50\text{-}100\ s^{-1}$), leading to a VDE directly after the thermal quench. Thus the VDE can be considered fast with respect to the current quench. The halo current fraction in both cases is similar at ~30% in spite of the slower VDE growth rate for the ILW case (see figure 6c). The toroidal asymmetry or Toroidal Peaking Factor (TPF) is in both cases approximately unity. Thus the force induced by the halo currents is expected to be the same. Previously (with C PFC) the reaction of the vessel was found to scale proportionally to the halo current [5]. A large difference is seen however in the reaction of the vessel to the applied force by the halo current, with a significantly larger reaction by the vessel for the ILW (i.e. the peak-to-peak value of the force swing shown in figure 6d).

The larger reaction force can directly be explained by the longer current quench phase, and thus the halo duration. The JET vessel characteristic time ($f_o \sim 14Hz$) is longer than the duration of most disruptions. Thus the vessel processes the force like a mass-damper-spring-system; creating the damped oscillations seen in figure 6d. The maximum displacement obtained in such a system is directly proportional to the force if this is applied continuously or for much longer than the natural frequency of the spring (the JET vessel). Hence one could express the vertical vessel displacement in units of an equivalent static force ($F_v$). For the JET vessel a static force of $F_v = 1MN$ is equivalent to a vessel excursion of about 1.3mm. However, for shorter impulses the maximum displacement can be much larger than the continuous application of a force of the same magnitude. A maximum is found when the impulse duration is resonant with the vessel characteristic time. For shorter durations, as is mostly the case for JET, the vessel reaction force would scale proportionally to the impulse, i.e. proportional to the time integrated halo force. Figure 7a shows that there is a spread of more than a factor of 2 in the reaction forces for disruptions that produce similar halo currents and TPF. A better correlation is found in figure 7b where Fv is plotted against the force impulse. Clearly the longer current quench duration can affect the reaction forces and vessel displacements due to disruptions, either for vertical displacements as discussed above, or radial displacements, as discussed elsewhere [13, 26].

### *3.3 MITIGATION BY MASSIVE GAS INJECTION*

The above results showed that mitigation of disruption heat loads and forces has become a necessity with the ILW. Massive Gas Injection has been a tested method for several years at JET [11]. In figure 4b it can be seen that MGI is capable of increasing the radiation fraction to near 100% with the ILW, thus significantly reducing the fraction of energy conducted to the PFCs and reducing the current quench duration. In figure 7 it is shown that the reduction in current quench duration for

MGI mitigated ILW disruptions resulted in a lower reaction force on the vessel, albeit not as low as found for natural disruptions with similar plasma configuration that occurred with C PFC (A more detailed analysis of MGI with the ILW is given elsewhere [27]).

MGI was previously never applied at JET as an active mitigation technique, i.e. used in a closed-loop protection system, triggered by real-time warning signs. In order to avoid further melt damage and to reduce the large vessel reaction forces seen for unmitigated ILW disruptions, MGI has been used for the first time as part of an active protection system at JET. It has become an obligatory for all operations with $I_p \geq 2.5$MA. Since the first use MGI as part of an active protection system, more than 35 high current disruptions have been mitigated. It should be noted that the effectiveness of the total system depends, besides the MGI efficiency to increase the fraction of radiation, also on appropriate warning signs/signals and the reaction time. So far, in all cases the gas reached the plasma after the thermal quench but during the current quench. As discussed in the introduction it is possible that a fast quench at high thermal energy could result in melt damage too. The intentional VDE shown in figure 5 shows two temperature maxima, the first linked to the fast thermal quench the next the slower dissipation of a larger amount of magnetic energy. For most unintentional, natural, disruptions, this has not been an issue up to know as the thermal energy was degraded significantly prior to the onset of such disruption. This either due to MHD activity that affected the confinement, too high radiation due to impurities (as shown in figure 1) or simply because other warning signs had initiated for example the shut-down of auxiliary heating systems. However, for high performance operations, foreseen in the future, the trigger for the MGI protection has to be optimised in order to also mitigate the thermal quench of high thermal energy plasmas.

## 4. OUT-GASSING AND DECONDITIONING

Disruptions can lead to significant degradation of the tokamak conditioning. For operations with C PFCs, conditioning at JET was usually obtained by baking of the vessel, glow-discharge cleaning or Be evaporation. Frequent glow-discharge cleaning was carried out during weekends [29]. The impact of a disruption could be noticed in the subsequent discharge by an increased recycling, and higher impurity content, yielding performance (i.e. confinement) degradation. Moreover, in quite a few cases it prevented plasma formation or breakdown entirely. Over the last 2 years of operation with C PFCs, it was found that 27% of all first breakdown attempts, following a disruption, failed, yielding a significant loss of operational time. Sometimes, additional conditioning, using the aforementioned techniques, had to be applied to regain plasma.

Important for the deconditioning due to disruptions, is their impact on the PFC and the resulting release of material, either hydrogen isotopes or impurities, retained by the wall. The outgassing can be quantified by the peak pressure seen in the vessel after the discharge [30]. A comparison of out-gassing by disruptive and non-disruptive discharges during both C and ILW operation is shown in figure 8. As expected the out-gassing for disruptive discharges is significantly larger than for non-disruptive cases. More interestingly, with the ILW the disruptive out-gassing has dropped by about 1 order of magnitude on average. This indicates that the reservoir of material that can be

released by disruptions is smaller with the ILW. The reverse is seen for non-disruptive discharges, for which the ILW shows a slightly higher out-gassing compared to C PFCs. This is consistent with a lower long-term retention (i.e. less stays behind after the discharge) [23]. Residual gas analysis has revealed that the composition of the gases released by the ILW is characterised by much lower C and O levels (1 order of magnitude) compared to C PFCs. With the ILW no breakdown failures attributable to deconditioning have occurred so far making operations more efficient. This statement covers all disruptions including those that were mitigated by MGI. The question as to what extent MGI affects the general plasma performance will not be addressed here.

Radiation spikes are observed in some ILW pulses and have been shown to be caused by particles of W, the most common, but also by particles of Ni or Fe which enter the plasma. A correlation has been found between the influx of micro-particles and the preceding disruptions with the ILW. The influx of these particles was detected and counted using radiation spikes. Such particles occurred in about 25% of all discharges following a disruption which is almost 7 times the average. The occurrence of these impurity influxes was also found to drop over time, during the progress of the experimental campaigns, the opposite trend to that of disruption frequency which increased. This indicates that disruptions do not form the micro-particles, but more likely redistribute existing particles, making them accessible to subsequent discharges. Over time, more and more of these particles must have reached locations from which even disruptions could not move them. Most discharges survived these radiative micro-particles. Their occurrence during the first phase of operation with the new wall is similar to that with C PFC.

Dust particles can be observed after disruptions, using the JET High Resolution Thomson Scattering diagnostic [31]. Plasma facing material can be eroded and re-deposited creating unstable surface layers which can be converted into dust particles by large thermal or mechanical loads [32]. As discussed above, unmitigated disruptions could conduct significant energies to the ITER-like wall, as only part of the total energy is radiated. But the erosion and dust formation can also take place during limiter operation. After the disruption laser-light used by the diagnostic is scattered by particles in the Tokamak vessel. It is difficult to determine whether the amount of scattered light is due to a few big particles or a larger number of smaller particles. For a rough comparison here the total amount of scattered light per disruption is used as a measure of the amount of dust seen after a disruption. For both C PFC and ILW operation the amount of scattered light from dust particles was found to increase with the vessel reaction force as shown in figure 9. The comparison in figure 9 also showed that the amount of dust observed with the new metal wall is a factor of 10 lower compared to the levels seen during the last 2 years of C PFC operations. Up to now there is no indication of an increase in the detected dust level during the ongoing operations with the ILW. ILW plasmas are much cleaner than their C PFC counter parts with typical $Z_{eff}$ in H-mode in in the range 1.2-1.4 with ILW compared to 1.8-2.5 with C PFCs. Cleaner plasmas means less material migration and so slower growth of deposits that can be converted into dust.

## CONCLUSIONS

The new JET ITER-like Wall has had a significant impact on disruption physics at JET. The strong reduction of C concentration seen from the very first ILW discharges has two direct consequences Firstly, the onset of the disruptive 'density-limit', the MARFE development, occurs at lower divertor temperatures, well below the optimum temperature for C radiation, and thus it is possible to achieve higher line-averaged plasma densities. Secondly, lower radiation and higher temperatures are observed during unmitigated ILW disruptions which lengthen the current quench phase, increase the impulse and result in a larger fraction of the total energy being conducted to the wall which is vulnerable to melting.

A clear distinction between the non-disruptive H-mode density-limit, resulting in a confinement back-transition to L-mode, and the disruptive L-mode density limit was found. Triggering such disruptions with the ILW required significant higher gas dosing (factor 5) compared to C PFC operation. It suggests that impurity radiation losses at the edge are more relevant to the process that drives the plasma unstable than recycling and re-ionization losses [22].

Typical current quench times suggest that for C PFCs, the temperatures after the thermal quench would have been merely several tens of eV and close to the optimum temperature for C radiation. The influx of wall material due to the heat pulse of the thermal quench impacting on the C PFC could be seen as self-mitigating in this case, increasing the impurity content, radiative fraction, lowering the temperature and thus enhancing the current quench rate. This does not take place with the ILW because of the absence of carbon. In several cases, flux surfaces were restored after the thermal quench, radiation levels remained low and Ohmic power could even restore the plasma temperatures, yielding longer current quench phases. VDEs have, even at low current ($I_p = 1.5$MA, $E_{tot} = 7$-8MJ), caused Be melt damage as a result of heat loads associated with the dissipation of magnetic energy. High heat loads due to fast thermal quenches in high performance discharges could also pose an additional problem but have so far not occurred during the first operations with the ILW. The longer current quench time resulted in a larger reaction forces and vessel displacements. Active mitigation by MGI therefore became a necessity for ILW operations both because of heat loads and forces. For the first time it has been applied as an active protection system at JET. On the positive side, the longer current quench rates and thus lower toroidal electric fields have made it more difficult to generate runway electron beams.

Cleaner machine conditions after the installation of the ILW are indicated by lower dust levels and fewer influxes by high Z micro-particles. Disruptions with the ILW, unmitigated and even those mitigated by MGI, were found to have a negligible impact on the following discharge. So far no cases have been found where the plasma formation failed because of deconditioning due to disruptions. A lower fraction of non-sustained breakdown failures made JET operations, and especially dedicated disruption experiments, more efficient.

## ACKNOWLEDGEMENT

This research was funded partly by the European Communities under the contract of Association

between EURATOM and FOM and was carried out within the framework of the European Fusion Development Agreement. The views and opinions expressed herein do not necessarily reflect those of the European Commission.

**REFERENCES**

[1]. T.C. Hender et al 2007 Nuclear Fusion **47** S128
[2]. M. Sugihara et al 2007 Nuclear Fusion **47** 335
[3]. F.C. Schüller 1995 Plasma Physics and Controlled Fusion **37** A135
[4]. P.C. de Vries et al 2011 Nuclear Fusion **51** 053018
[5]. V. Riccardo et al 2004 Plasma Physics and Controlled Fusion **46** 925
[6]. V. Riccardo et al 2005 Nuclear Fusion **45** 1427
[7]. G. Arnoux et al 2009 Nuclear Fusion **49** 085038
[8]. D.G. Whyte et al 2002 Physical Review Letters **89** 055001
[9]. R.S. Granetz et al. 2007 Nuclear Fusion **47** 1086
[10]. G. Pautasso et al 2007 Nuclear Fusion **47** 900
[11]. M. Lehnen et al 2011 Nuclear Fusion **51** 123010
[12]. V. Philipps et al 2010 Fusion Engineering and Design **85** 1581
[13]. V. Riccardo et al 2010 Plasma Physics and Controlled Fusion **52** 124018
[14]. V. Riccardo et al 2002 Plasma Physics and Controlled Fusion **44** 905
[15]. K. Borrass 1991 Nuclear Fusion **31** 1035
[16]. K. Borrass et al 2004 Nuclear Fusion **44** 752
[17]. J. Rapp et al 2008 Plasma Physics and Controlled Fusion **50** 095015
[18]. G.R. Harris 1990 'Comparisons of the current decay during carbon-bounded and beryllium bounded disruptions in JET' JET-R (90) 07
[19]. R. Dux et al 2007 Journal of Nuclear Materials **363–365** 112
[20]. P. Buratti et al 1997 Plasma Physics and Controlled Fusion **39** (1997) B383
[21]. M. Greenwald 2002 Plasma Physics and Controlled Fusion **44** R27
[22]. A. Huber et al 2012 'Impact of the ITER-like Wall on Divertor Detachment and on the Density Limit in the JET Tokamak' 20th conference on Plasma Surface Interaction (2012 Aachen), submitted to Journal of Nuclear Materials (2012)
[23]. S. Brezinsek et al 2012 submitted to Plasma Physics and Controlled Fusion **54** 00000
[24]. V. Riccardo et al. 2005 Plasma Physics and Controlled Fusion **46** 117
[25]. M.N. Rosenbluth and S.V. Putvinski 1997 Nuclear Fusion **37** 1355
[26]. S. Gerasimov et al 2012 'The Rotation of Plasma Current Asymmetries during Disruptions in JET' 38th EPS conference on Plasma Physics (2012, Stockholm)
[27]. M. Lehnen et al 2012 'Impact and mitigation of disruptions with the ITER-like wall in JET' 20th conference on Plasma Surface Interaction (2012 Aachen), submitted to Journal of Nuclear Materials (2012)
[28]. S.P. Gerhardt et al 2012 Nuclear Fusion **52** 063005

[29]. D.Kogut et al 2012 'Study of JET conditioning with the ITER-like wall' 38th EPS conference on Plasma Physics (2012, Stockholm)
[30]. V. Philipps et al 2009 Journal of Nuclear Materials **78** 390
[31]. E. Giovannozzi et al 2010 Review of Scientific Instruments **81** 10E131
[32]. R. Neu 2011 Plasma Physics and Controlled Fusion **53** 124040

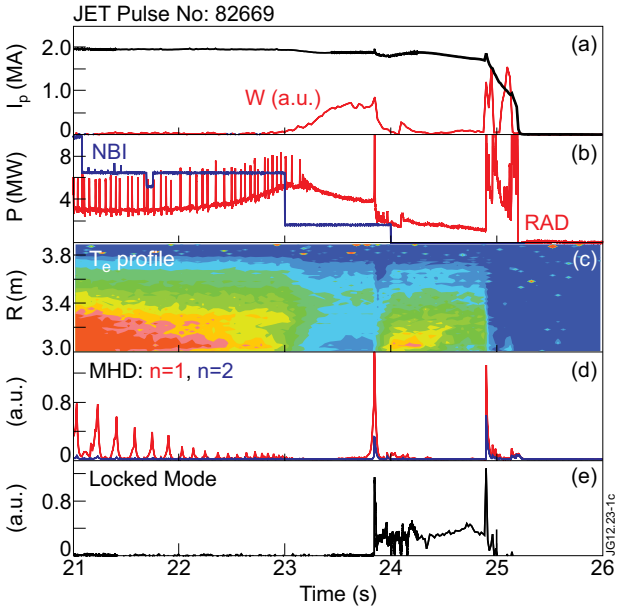


*Figure 1: Example of a disruption caused by impurity accumulation. a) The plasma current and core W spectroscopy intensity. b) The NBI and radiation power as measured by the bolometer. c) Contour plot of electron temperature (Te) profile from the core at R = 3.0m to the edge at R = 3.9m. The levels range from blue ($T_e$ = 0keV) to red at $T_e$ = 2keV d) The MHD activity with toroidal mode numbers n = 1 and n = 2. e) The amplitude of the locked mode.*

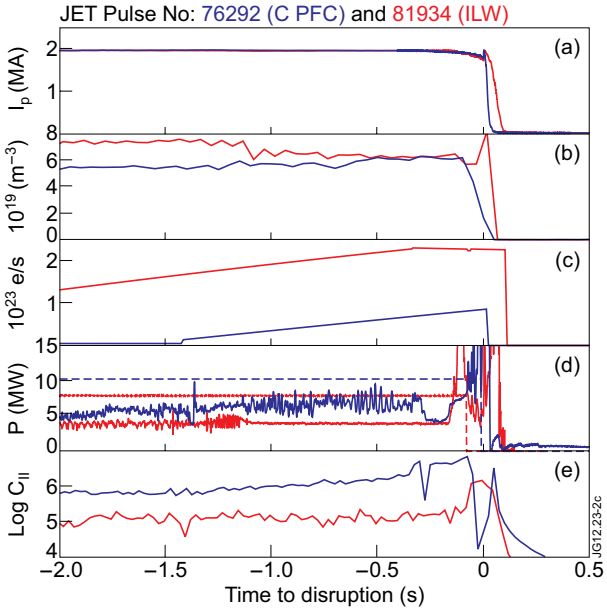


*Figure 2: Comparison of density limit disruptions with C PFC and the ILW with similar main parameters $B_T$ = 3.1T, $I_p$ = 2.0MA, $q_{95}$ = 4.5, a high triangularity configuration with $<\delta>$ = 0.42 in ELMy H-mode using $P_{NB}$ = 8-10MW. a) The plasma current as a function of the time to the disruption, indicated by the current spike at t = 0s. b) The line-averaged density. c) The deuterium dosing rate in electrons per second. d) The NB powers for both pulses (dashed) and the radiation powers. e) The logarithmic of the CII line-intensity (90.4nm) in a.u.*

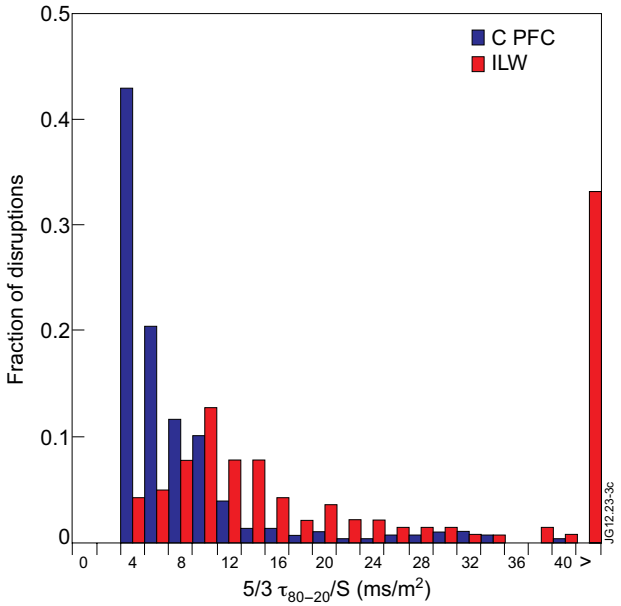


*Figure 3: Statistical comparison of the current quench times 5/3 $t_{80-20}$/S for C PFC and ILW operations. The statistics are based on all 308 unintentional disruptions over the C PFC period 2008-2009, that did not exhibit runaway formation, and 142 unintentional disruptions for the first operations of the ILW in 2011 and 2012, that were not mitigated by massive gas injection.*

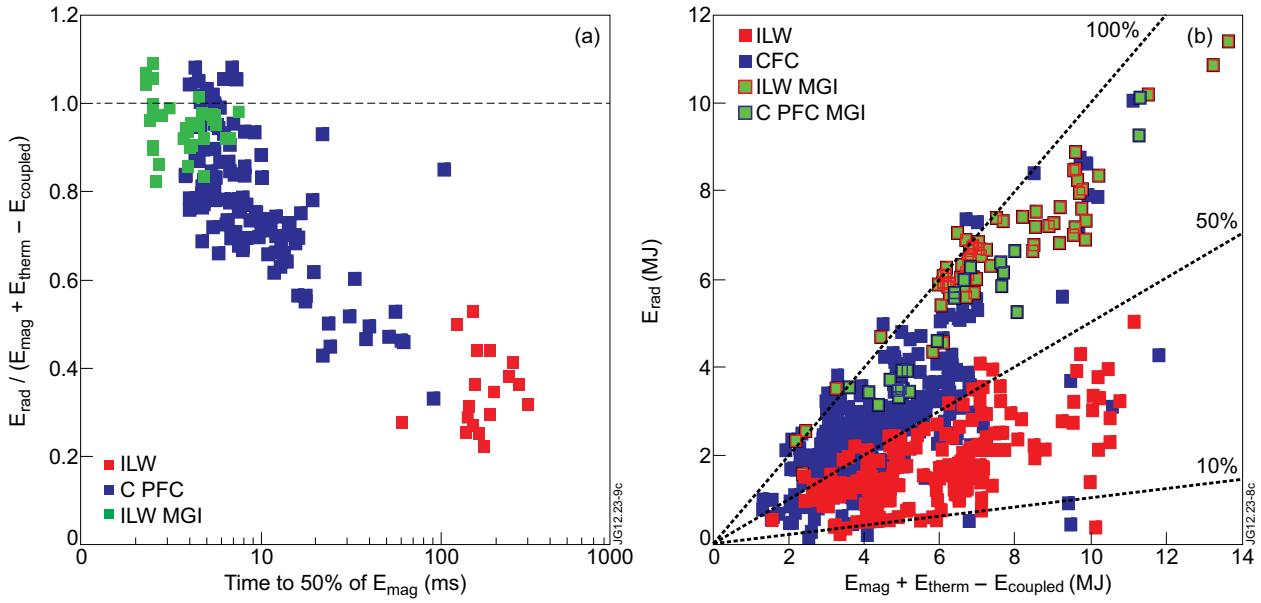


*Figure 4: a) The fraction of energy not coupled back into the toroidal conductors, that is radiated during the current quench versus the time it takes to reduce the magnetic energy ($\propto I_p^2$) to 50%. b) The total energy radiated during the current quench phase versus the part of the total energy that is not coupled back into the toroidal conductors.*

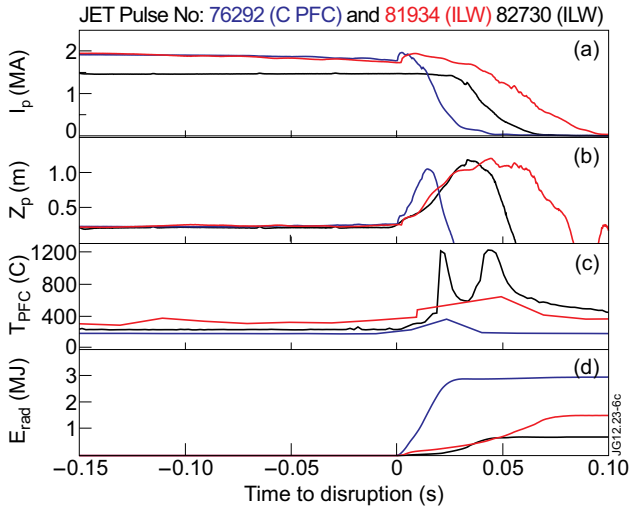


*Figure 5: a) The plasma current for 3 discharges; two density limit disruptions with C PFC and the ILW, shown in figure 2 and an intentionally triggered VDE with the ILW, at lower plasma current, shown in black. b) The vertical position. c) The maximum temperature measured in the upper part of the vessel (upper-dump plates, upper inner-wall protection). This does not necessarily have to be at the same location in time. Note that the vessel operating temperature at JET is 200°C. d) The total radiated energy during the current quench phase.*

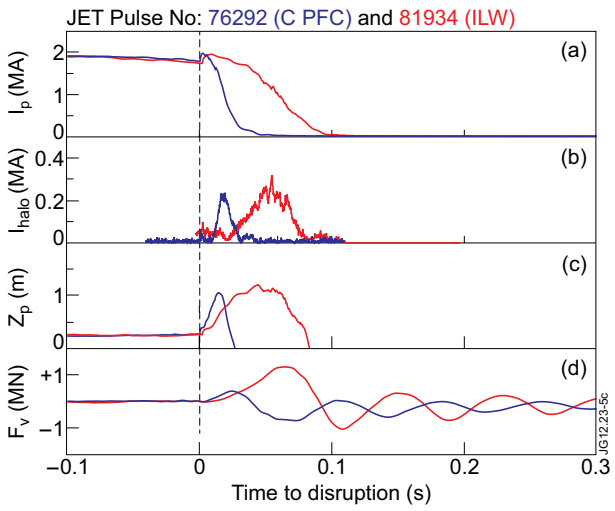


*Figure 6: Comparison of halo currents and vessel reaction forces induced due to the two density limit disruptions with C PFC and the ILW, shown in figure 2. a) The plasma current as a function of the time to the disruption, i.e. the thermal quench at t = 0s. b) The average halo current measured by coils at the upper part of the vessel. c) The vertical plasma position, indicating the vertical displacement event (VDE) that develops after the thermal quench. d) The measured dynamic reaction force of the JET vessel.*

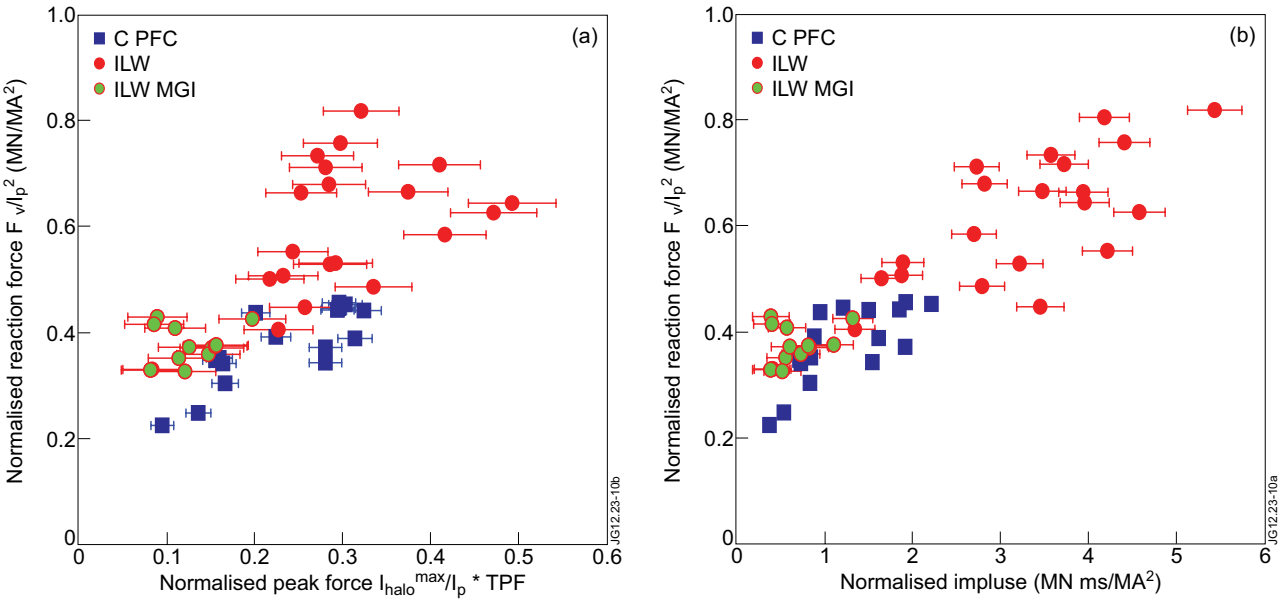


*Figure 7: a) The equivalent static force required for the measure vessel excursion normalised to the plasma current squared versus the normalised halo current force, similar as presented in [5] for a set of high triangularity C PFC and ILW disruptions. b) The same parameter versus the time integrated halo force or impulse also normalised to the plasma current. Those ILW disruptions mitigated by means of MGI are separately labelled.*

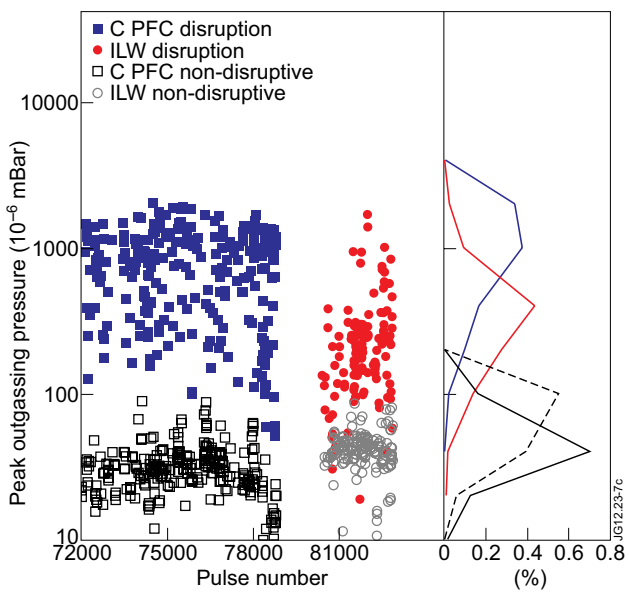


*Figure 8: The peak pressure in the Tokamak measured after the discharge with penning gauges which indicates the amount of out-gassing, for all un-intentional disruptions ($I_p$ > 1MA) over the period 2008-2009 (C PFC Pulse No's: 72003-78806) and 2011-2012 (ILW Pulse No's: 80128- 82881). These are compared with a series of undisruptive examples. Discharges performed in He or without cryogenic divertor pumping or disruptions that were mitigated by MGI are not shown.*

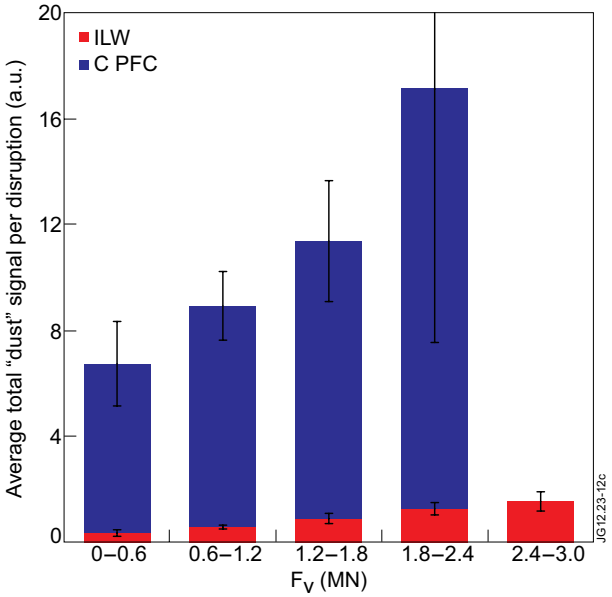


*Figure 9: The average amount of dust per disruption as a function of the vessel reaction force due to disruptions. Here the amount of dust is defined as the total integrated laser-light scattered by material in the vessel, seen by the JET High-resolution Thomson Scattering Diagnostic, after a disruption. The integration is done over all radial channels and over the duration of the signal. Larger error bars are found for the C PFC data because of the larger variation of the data per disruptions in each bin, especially for the bin $F_v$ = 1.8-2.4MN.*